Inorganica Chimica Acta 514 (2021) 119984

Contents lists available at ScienceDirect

Inorganica Chimica Acta

journal homepage: www.elsevier.com/locate/ica

Research paper

Sequence-specific assignments in NMR spectra of paramagnetic systems: A non-systematic approach

Inês B. Trindade[a], Michele Invernici[b], Francesca Cantini[b], Ricardo O. Louro[a,*], Mario Piccioli[b,*]

[a] Instituto de Tecnologia Química e Biológica António Xavier (ITQB-NOVA), Universidade Nova de Lisboa, Av. da República (EAN), 2780-157 Oeiras, Portugal
[b] Magnetic Resonance Center and Department of Chemistry, University of Florence, Via L. Sacconi 6, 50019 Sesto Fiorentino, Italy

ARTICLE INFO

Keywords:
Paramagnetic NMR
Metalloproteins
Biological inorganic chemistry
Metal ion in biological systems
HIPIP
Iron-sulfur proteins

ABSTRACT

The complete assignment of ^{1}H, ^{13}C and ^{15}N protein signals, which is a straightforward task for diamagnetic proteins provided they are folded, soluble and with a molecular mass below 30,000 Da, often becomes an intractable problem in the presence of a paramagnetic center. Indeed, the hyperfine interaction quenches signal intensity; this prevents the detection of scalar and dipolar connectivities and the sequential assignment of protein regions close to the metal ion(s). However, many experiments can be optimized and novel experiments can be designed to circumvent the problem and to revive coherences invisible in standard experiments. The small HiPIP protein PioC provides an interesting case to address this issue: the prosthetic group is a $[Fe_4S_4]^{2+}$ cluster that is bound to the 54 amino acids protein via four cysteine residues. The four cluster-bound cysteine residues adopt different binding conformations and therefore each cysteine is affected by paramagnetic relaxation to different extent. A network of tailored experiments succeeded to obtain the complete resonance assignment of cluster bound residues.

1. Introduction

Since Luigi Sacconi and the golden age of coordination chemistry [1], the presence of a paramagnetic center has represented a challenging opportunity for NMR spectroscopists [2–7]. The Zeeman interaction between electron spin and nuclear spins originates contributions to chemical shifts and relaxation rates of those nuclear spins sensing the electron spin. On the one hand, these shifts and relaxation properties provide information on the coordination geometry of the metal center (number and type of ligands and coordination mode) and on the electronic properties of the metal center at room temperature. On the other hand, the line broadening induced by paramagnetic relaxation disturbs communication between nuclear spins and eventually prevents the detection of these signals [8–10].

The growing interest for metal ions in biology and the advent of high field NMR spectrometers contributed to maintain, for decades, the interest in NMR of paramagnetic systems. In paramagnetic metalloproteins, the consequences of the hyperfine interaction are manifolds. In the presence of a paramagnetic center, the complete assignment of ^{1}H, ^{13}C and ^{15}N protein signals, nowadays a straightforward task for diamagnetic proteins provided they are folded, soluble and with a molecular mass below 30,000 Da [11–14], often becomes a jigsaw puzzle, in which several pieces of the puzzle are missing. When both coherence transfer and cross relaxation effects are not observed because signal intensities are quenched due to the hyperfine interaction, the sequential assignment is not possible. In the case of proteins uniformly enriched with ^{15}N and ^{13}C, the sequence specific assignment strategy of NMR signals is based on scalar connectivities that are obtained via a battery of standard triple resonance experiments and eventually supported by NOESY-type experiments. The latter are usually redundant, so that when some piece of information is missing in any of the standard experiments, it is still possible to achieve the complete NMR assignment with a systematic approach.

The quench of NMR information due to a paramagnetic center is not randomly distributed throughout the entire protein frame but is localized in a sphere, usually called “blind sphere”, around the paramagnetic center [15,16]. When the protein backbone falls within the blind sphere, the sequential connectivities may be lost. The assignment is then available only for residues outside the sphere where the paramagnetic effect is dominant. Many efforts and many instrumental and technological developments over the last twenty years contributed to develop experiments tailored to the identification of signals affected by the hyperfine interaction and to “revive” coherences invisible in standard experiments [17]. In order to obtain a complete NMR assignment, the automated sequence specific assignment protocol must be complemented with a non-systematic approach where experiments are

* Corresponding authors.
E-mail addresses: louro@itqb.unl.pt (R.O. Louro), piccioli@cerm.unifi.it (M. Piccioli).

https://doi.org/10.1016/j.ica.2020.119984
Received 6 July 2020; Received in revised form 14 August 2020; Accepted 23 August 2020
Available online 28 August 2020

optimized to circumvent the loss of information due to paramagnetic relaxation. Each experiment should be performed using customized acquisition and processing parameters and *ad hoc* pulse sequences, in order to minimize the loss of information arising from paramagnetic relaxation. Since paramagnetic relaxation depends on the nucleus investigated [18] and on the metal-to-nucleus distance [19], also the assignment strategy needs to be defined according to the structural properties of the system investigated, that is why we termed this as a "non-systematic" approach. As we will show throughout this article, four cysteine residues bound to the same paramagnetic center with different coordination topologies will be assigned using, for each of them, a different combination of tailored NMR experiments.

It is worth noting that paramagnetic NMR represents nowadays a toolkit with many applications in structural biology [20] and material science [21]. Used to induce orientation, or relaxation or shifts, the binding of paramagnetic tags at specific protein sites contributes to address protein structures [22,23], protein–protein interactions [24–26], RNA [27], invisible states [28–30], membrane proteins [31], intrinsically disordered proteins [32–34], drug discovery [35], in-cell NMR [36,37]. On the one hand, *ab-initio* calculations of paramagnetic shifts and susceptibility, contributed to design *ad-hoc* paramagnetic probes and to compute paramagnetism-based structural restraints [38–41]; on the other hand relaxation anisotropy [42,43], intermolecular interactions [44], cross correlations [45–47], charge delocalization [48], still pose questions on the accuracy of paramagnetic relaxation as structural restraints. Methodological aspects play a non-marginal role in this scenario: new experiments have been recently developed to accurately measure relaxation rates greater than 100 s^{-1} [49,50]. The quantification of shift and relaxation properties of a small number of additional signals may become the key to unravel a reaction mechanism [51,52].This is why a small and stable paramagnetic protein is an ideal test case to verify the efficiency of a given experimental approach. The case study presented here is a High Potential Iron-sulfur Protein (HiPIP), consisting of 54 amino acids and a $[Fe_4S_4]^{2+}$ coordinated by cysteine 22, cysteine 25, cysteine 34, and cysteine 47, as represented in Fig. 1.

HiPIPs are a class of small electron-transfer proteins, characterized by a small polypeptide chain (54–90 aa) bound to a $[Fe_4S_4]^{3+/2+}$ cluster [53]. The CD spectrum of PioC (Fig. 1) shows features characteristic of a folded protein with a small content of a-helix, as indicated by two negative bands at 222 and 209 nm and the absence of the minimum at 198 nm typical of random coil segments. This is consistent with the absence of secondary structure elements and with a protein fold essentially driven by the [4Fe-4S] cluster. Three peculiarities of HiPIPs are relevant for this study: i) a large fraction of the protein (especially for the smallest protein of the series) is wrapped around the cluster and therefore it is affected by paramagnetic relaxation; ii) cysteines bind the cluster adopting different conformations, given by the χ_1 and χ_2 dihedral angles [χ_2 is the C_α-C_β-S_χ -Fe solid angle] and also by the orientation of CO, HN and $H_\alpha C_\alpha$ dipoles. Therefore, the consequences of paramagnetism on all Cys resonances (C', C_α, C_β, N, H_N H_α,H_β) depend on the local conformation; iii) $[Fe_4S_4]^{2+}$ have negligible magnetic susceptibility anisotropy and we expect that nuclei in the proximity of the cluster but not directly bound to it, will experience substantial paramagnetic relaxation effects but small/negligible contributions to the chemical shifts. This situation represents the most challenging case for the assignment, because many signals are broadened and buried within the diamagnetic envelope. The optimized protocol verified here would be the basis for the study of more complex and unstable proteins, such as those of the iron-sulfur cluster assembly machinery.

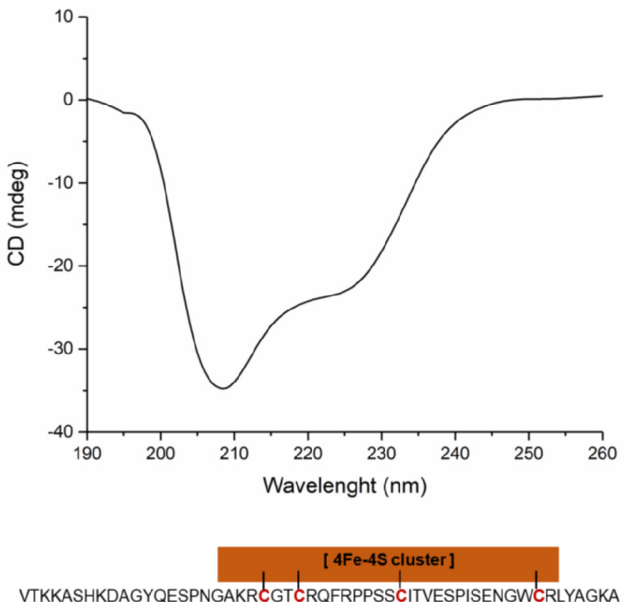

Fig. 1. Primary sequence and CD spectrum of PioC.

2. Materials and methods

2.1. Protein expression and purification

Unlabeled, ^{15}N labeled and ^{15}N,^{13}C labeled PioC samples were expressed as described elsewhere [54]. The lysate was ultra-centrifuged at 204709g for 90 min at 4 °C and the supernatant was dialyzed overnight against 50 mM potassium phosphate buffer pH 5.8 with 300 mM NaCl before injection in a His-trap affinity column (GE Healthcare). The fraction containing Histag-PioC eluted with 250 mM imidazole and was incubated overnight with Thrombin (GE Healthcare) for digestion. After removing the imidazole, a 2nd passage through the His-trap column was performed to remove the His-tagged protein. The purity of untagged PioC was confirmed by SDS-PAGE with Blue Safe staining (NzyTech) and by UV–Visible spectroscopy. Final protein concentration was approximately 0.5 mM.

Circular Dicroism Measurements. Circular dicroism spectrum of PioC (35 uM) was obtained over a wavelength range from 190 to 260 nm, at a scan rate of 50 nm/min and a response time of 1 *sec* in a quartz cuvette of 1.0 cm path length using Jasco J-810 CD spectropolarimeter. The spectrum was acquired with an accumulation of 30 scans. Temperature control within the CD instrument was done using the Peltier temperature control device that is integrated within our instrument

2.2. NMR experiments

Double and triple resonance ^1H detected experiments were recorded using Bruker AVANCE-NEO spectrometers operating at 700 MHz and 500 MHz, equipped with cryogenically cooled triple resonance inverse detection probeheads (CP-TXI). ^{13}C-detected experiments, collected on an AVANCE-NEO 700, were acquired at 176.05 MHz using a cryogenically cooled probe-head optimized for ^{13}C direct detection (CP-TXO). ^1H experiments were recorded at 400 MHz using a room temperature, selective 5 mm ^1H probe without pulsed field gradients, designed for the acquisition of large spectral windows. All spectra were processed using the Bruker software TopSpin.

Proton resonances were calibrated with respect to the signal of 2,2-dimethylsilapentane-5-sulfonic acid (DSS). Nitrogen chemical shifts were referenced indirectly to the ^1H standard using a conversion factor derived from the ratio of NMR frequencies. Carbon resonances were calibrated using the signal of dioxane at 69.4 ppm (298 K) as secondary reference.

HNCA experiments were performed as 2D experiments. Data matrices of 1024x160 data points were acquired, using 512 scans for each

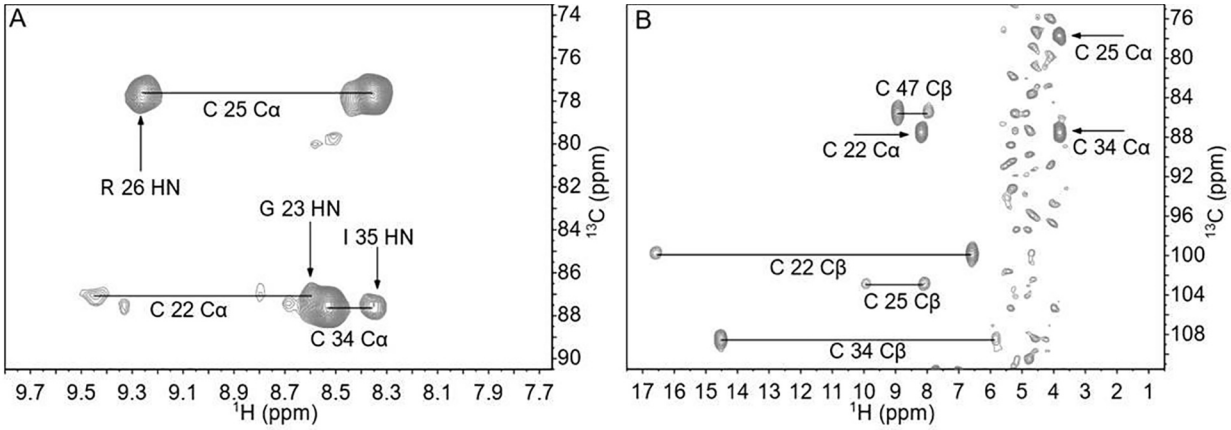

Fig. 2. 500 MHz 298 K, H(N)CA (A) and ^{13}C HSQC (B) spectra of PioC optimized for peaks involving fast relaxing resonances. The ^{13}Cα shift values allows the sequential assignment of three out of the four cluster-bound cysteines in the HNCA, while the βCH$_2$ pairs are unambiguously identified via ^{13}C HSQC.

fid and 0.5 s recycle delays. ^{13}C- and ^{15}N-HSQC experiments were acquired with 1024x256 data point matrices using 1024 (^{13}C) and 256 (^{15}N) scans for each fid and 0.15 s recycle delays. In both cases, ^{1}H signals were acquired as antiphase doublets without decoupling during acquisition [55].

1D NOE experiments were collected over an 80 ppm spectral window using a superWEFT [56] pulse sequence with 110 ms and 133 ms as inter-pulse and acquisition delays, respectively. About 500.000 scans for each experiment were performed. Selective saturation was applied during the inter-pulse delay to achieve steady state, each signal was suppressed ca 50–70% of its initial intensity. Experiments were acquired in an interleaved way with an experiment in which selective irradiation was applied off resonance [57,58].

One dimensional ^{13}C experiments were performed without ^{1}H decoupling. A short, hard pulse was used to excite the full ^{13}C spectrum. 32768 scans were recorded, using a 75 ms recycle delay. A ^{13}C–^{13}C COSY experiment was performed as previously described [59]. A 2048x512 data point matrix was acquired, over 258 ppm spectral windows. About 480 scans for each fid were collected, using 22 ms and 200 ms as acquisition and recycle delays, respectively. The final 2D spectrum used for assignment was obtained by considering only a 1500x400 data point matrix, apodized with sine bell function before Fourier transformation.

3. Results

3.1. Paramagnetism-tailored HNCA and ^{13}C HSQC experiments

In order to identify signals affected by the hyperfine interaction, we recorded a paramagnetic-tailored HNCA experiment. The spectral windows of ^{1}H, ^{15}N, ^{13}C$_\alpha$ and ^{13}C' spins are critical parameters that need to be adjusted: when the paramagnetic center is a $[Fe_4S_4]^{2+}$ center, the hyperfine shift arises only from the contact contribution due to unpaired electron delocalization [17]. Therefore, ^{13}C$_\beta$ and ^{13}C$_\alpha$ spins, that are respectively two and three sigma bonds away from the iron ions, will likely experience a sizable hyperfine shift, typically consisting of about 50–90 ppm for ^{13}C$_\beta$ and 15–35 ppm for ^{13}C$_\alpha$ atoms. *En-revanche*, ^{1}H$_\alpha$, ^{15}N and ^{13}C', that are four sigma bonds away from the paramagnetic center, will be affected at much lower extent, if any. Therefore, to obtain a paramagnetic HNCA we should move the ^{13}C$_\alpha$ carrier from 53.5 ppm, which we take as reference value for a diamagnetic HNCA, to about 85 ppm, while the other spectral windows of the experiments remain the same of a standard experiment. Then, the optimization of the INEPT and the inverse INEPT steps of the experiment is crucial. The coherence transfer delay responsible of the H—N scalar coupling evolution, typically 5.5 ms i.e. 1/(2J$_{HN}$), must be shortened to about 1.0–2.0 ms. This is due to the fact that magnetization H$_x$N$_z$ relaxes with ^{1}H T_2, which is highly sensitive to paramagnetic relaxation enhancements [49]. Counter-intuitively, the long delay for the N to Cα transfer, typically 45 ms, does not require a strong reduction. Indeed, during the N to C$_\alpha$ INEPT transfer, and back transfer, ^{1}H$_N$ and ^{13}C$_\alpha$ spins are on the z axis and the only in-plane magnetization is N$_x$. The Solomon equation has a γ^2 dependence [19]; therefore paramagnetic relaxation is very much dependent on the active nucleus [15,18,60–64]. Given the same metal-to-nucleus distance, the paramagnetic relaxation enhancement is 16 times smaller for ^{13}C spins and 100 times smaller for ^{15}N spins than the ^{1}H case [65]. Therefore, during a triple resonance experiment, the critical steps are those where the ^{1}H magnetization is on the xy plane and therefore it is relaxing with ^{1}H T$_2$, while the N to C$_\alpha$ INEPT is relatively unaffected by the paramagnetic effects. Other crucial modifications of the standard experiment are the removal of other elements that contribute to increase the overall duration of the experiment: the selective ^{1}H 180° pulses used for watergate, the use of 1 ms long gradients, the echo-antiecho quadrature detection scheme. Indeed, all these blocks require additional delays where ^{1}H$_N$ magnetization is on the xy plane [66]. Short acquisition times and recycle delays are also required. Short acquisition time has a multiple role: on the one hand, its reduction must be coherent with the decrease of recycle delay in order not to change the duty cycle of the experiment; on the other hand, fast relaxing signals disappear after a few millisecond of acquisition, therefore there is no need to acquire the NMR signal up to 100 ms, as it is typically the case of standard experiments. The use of fast repetition rates is a requirement not only to increase the number of scans, that are always needed when dealing with paramagnetic signals, without increasing the overall experiment time, but also because fast repetition is efficient to suppress the solvent peak because of progressive saturation. The very same concepts are used to optimize the ^{13}C HSQC experiment. The paramagnetic tailored HSQC experiment has been performed using 1.2 ms instead of the 3.3 ms of the standard set-up, without the constant time evolution during the ^{13}C dimension, removing the inverse INEPT step and without any ^{13}C decoupling.

Thanks to the paramagnetism-tailored HNCA experiment (Fig. 2**A**), H$_N$, N$_H$ and C$_\alpha$ resonances of Cys22, Cys25 and Cys34 have been assigned due to the sequential connectivities observed with HN signals of residues Gly23, Arg26 and Ile35. Arg26 and Ile35 are unambiguously identified with the standard assignment strategy; Gly23 has not been sequence specifically assigned because it belongs to the two-residue fragment between Cys22 and Cys25. However, the C$_\alpha$ shift, unambiguously identified in a standard HNCA experiment, allow us to assign the HN signal at 8.62 ppm as due to a Glycine residue, and the only cysteine residue followed by a Glycine is, indeed, Cys22. Fig. 2**B**

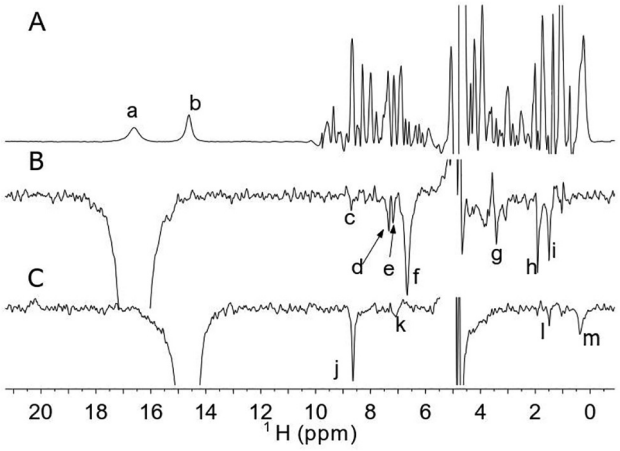

Fig. 3. A 1D ^{1}H NMR spectrum of PioC, optimized to observe hyperfine shifted and fast relaxing resonances. Two isolated peaks (labeled a-b) are observed. **B–C** 1D NOE difference spectra obtained upon selective saturation of signals at 16.0 ppm (B) and 14.5 ppm (C). The NOE peaks observed in the difference spectra, labeled c-m, are used to perform the assignment of signals a and b. Experiments were performed at 400 MHz and 298 K.

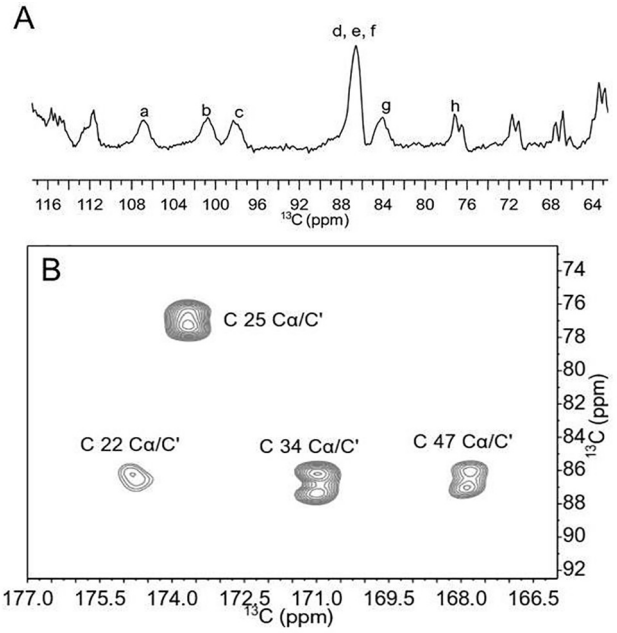

Fig. 4. A 1D ^{13}C NMR spectra of PioC, optimized to observe fast relaxing resonances. Figure shows the spectral region where we expect to observe $^{13}C_\beta$ and 13Cα of cluster-bond residues. **B** Upper diagonal part of a ^{13}C-^{13}C COSY spectrum of PioC showing the connectivities between C' and Cα signals. Acquisition and processing parameters are optimized to identify connectivities among fast relaxing resonances.

shows a paramagnetic ^{13}C-HSQC-AP experiment. The Anti-Curie temperature dependence (data not shown) confirms the identification of 4-βCH$_2$ and 3-αCH of the ligand cysteines. Through the cross peaks obtained in the ^{13}C-HSQC and in the HNCA experiments, the H_α resonances of Cys22, Cys25 and Cys34 have been assigned.

^{1}H NMR and NOE Experiments. The use of one dimensional, steady state NOE experiments obtained upon selective saturation of hyperfine shifted signals is a well-established approach, extensively used, since the last century, by all NMR groups dealing with NMR spectroscopy of paramagnetic systems [58,67–74]. Far from being obsolete, 1D NOE experiments are still the most efficient experiment when one needs to identify as many as possible dipolar connectivities between signals belonging to the first coordination sphere and those of the immediate proximity. Indeed, a selective one-dimensional experiment allows one to optimize the signal-to-noise ratio and detect NOEs below 0.5%. NOE experiments are applicable only when there are well-isolated signals that can be selectively saturated [75]. Indeed, the ^{1}H NMR spectrum of PioC (Fig. 3**A**) contain two signals that experience downfield hyperfine shift (16.6 ppm and 14.5 ppm) with antiCurie temperature dependence and paramagnetic line broadening, showing the typical fingerprint of two H_β signals of cysteines bound to a $[Fe_4S_4]^{2+}$ cluster [76]. Moreover, signals **a** and **b**, at 16.6 and 14.5 ppm, have been identified as Cys H_β signals also in the ^{13}C-HSQC previously shown. Fig. 2B-2C show the NOE difference experiments performed upon selective irradiation of these two signals. They allow us to detect and measure Nuclear Overhauser Enhancements (NOEs) between these two protons and their environment. From the selective saturation of the H_β signal at 16.6 ppm (Fig. 3**B**), a strong NOE is observed with its geminal partner at 6.60 ppm (f). Other NOEs are observed with Gly23 H_N (c), with Arg21 H_β (h) and Arg21 Hγ (i). All these protons belong to the second coordination sphere of the cluster, they do not experience any hyperfine shift and therefore they have been assigned with the standard assignment protocol. This network of inter-residue connectivities unambiguously assign the signal at 16.6 ppm as the Cys22 $H_{\beta2}$ signal. Additionally, this NOE experiment also allows us to identify spatial proximity with H_δ and H_ε of Phe28 (e,f) and with Glu43 H_α (g). Upon irradiation of H_β signal at 14.5 ppm (Fig. 3**C**), a strong NOE is observed to the HN resonance of Cys34 at 8.55 ppm (j), already identified from the HNCA experiment and identifies the signal at 14.5 ppm as the $H_{\beta2}$ of Cys34. In addition, Cys34 $H_{\beta2}$ gives NOEs to H_α Val 37 (l) and Hγ Ile 41 (m). As an obvious consequence of these assignments, C_β signals of Cys22 and Cys34 can be attributed from the ^{13}C HSQC-AP experiment shown in Fig. 2**B**.

3.2. *^{13}C direct detection experiments*

The development of triple resonance NMR probes with the inner coil designed and optimized at cryogenic temperature for ^{13}C direct detection, represents one of the instrumental advancements that significantly contributed to the successful use of ^{13}C direct detection in paramagnetic systems [18]. Indeed, ^{13}C direct detection provides useful information, also in the 1D ^{13}C spectrum, shown in Fig. 4**A**. Signals belonging to Cys bound residues are expected to experience a strong anti-Curie temperature dependence. This allows us to confirm the assignment of Cys22 and Cys34 C_α and C_β signals and of Cys 25 C_α. Additionally, two other Cys C_β signals are observed at 111.1 and 102.65 ppm, consistent with the paramagnetic ^{13}C HSQC spectrum.

Two dimensional ^{13}C detected experiments have shown their potential over the last years, especially for intrinsically disordered proteins [77], systems in chemical exchange [78] and paramagnetic proteins [15,63,79,80]. In particular, the ^{13}C–^{13}C COSY is a very simple and powerful experiment. As previously shown [59], the choice of t_{1max}, t_{2max} and of the recycle delay can critically affect the identification of C_αC' connectivities in both upper and lower part of the diagonal in the COSY spectrum. A tailored choice for t_{1max} and t_{2max} values provided [59], for the upper diagonal part, the spectrum shown in Fig. 4**B**, which identified all C_α/C' connectivities of cluster bound cysteines. This allowed us to assign C' resonances of the four Cys residues, to confirm the assignment of C_α of Cys22, Cys25 and Cys34 and to identify the missing Cys47 C_α, unobserved in the 1D ^{13}C experiments because in overlap with Cys34 and Cys22 Cα and unobserved also in the ^{13}C-HSQC-AP experiment shown previously. The set of ^{13}C direct detected experiments is completed by a CON experiment [18]. A CON-based experiment has also been used to measure correlated chemical shift modulations in metalloproteins [78]. The version of the experiment tailored to the assignment shows the N(i)/C(i-1) connectivity

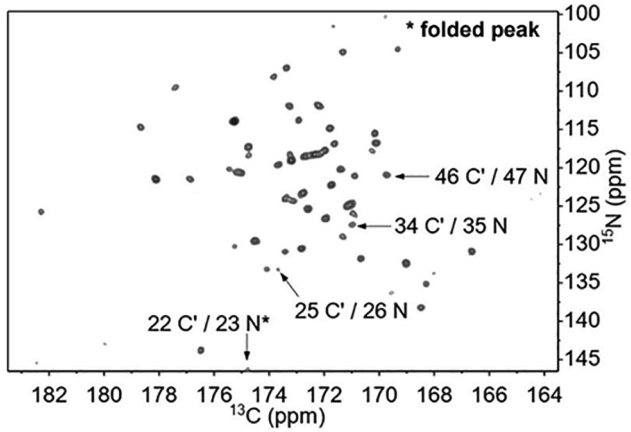

Fig. 5. 2D CON spectrum of PioC, collected at 175 MHz ^{13}C Larmor Frequency. Signals involving C' spins from cluster-bound cysteines are labeled in Figure.

observed via a C' to N INEPT transfer, which is quite robust with respect to paramagnetic relaxation enhancements, Fig. 5 confirms indeed the cysteine amide nitrogen assignment for Cys22, Cys25 and Cys34 and provides the assignment for the amide nitrogen of Cys47.

^{15}N HSQC experiments. We have already shown, in several paramagnetic proteins, that most of the HN peaks that are lost in a standard ^{15}N-HSQC experiment can be recovered when the INEPT HN delay is shortened and the inverse INEPT is replaced by the acquisition of ^{1}HN signals in antiphase mode [50,51]. This is in strict analogy with what was previously discussed in detail for the HNCA and the ^{13}C HSQC cases. The four cysteines HN peaks are shown in Fig. 6. Like the previous CON experiment, the identification of the HN peaks from Cys residues confirm the assignment obtained with HNCA and extend it to the assignment of the amide Cys47 HN, which escaped detection also in the "optimized" version of HNCA. This accounts for a very efficient R_2 ^{1}H relaxation of the Cys 47 H_N amide proton that would prevent the identification of its HNCA peak. Consistently, the H_N signal at 6.50 ppm has ^{1}H T_2 values of 5.1 ms, accounting for an HN belonging to the first coordination sphere of the cluster without any connectivity in triple resonance experiments. All of them are affected by paramagnetic relaxation; however, paramagnetism affects these four signals to different extent, as qualitatively observed here from the relative peak intensities in the ^{15}N-HSQC-AP experiment. Cys25 and Cys34 have relatively sharp H_N resonances, clearly observable in the paramagnetic optimized HNCA, suggesting a cysteine orientation in which the amide group is pointing far from the cluster. On the other hand, Cys22 HN is very weak

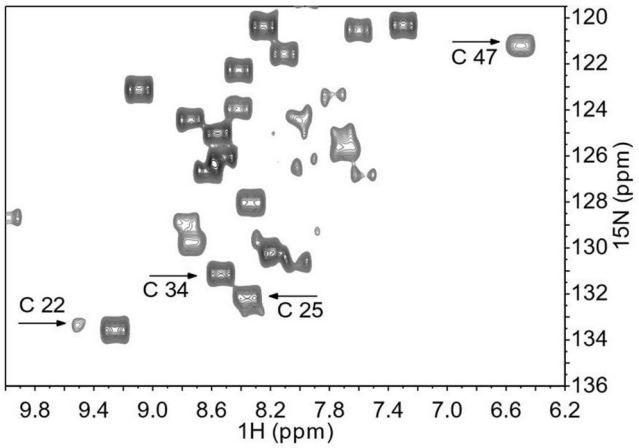

Fig. 6. Expanded region of a ^{15}N HSQC-AP spectrum of PioC where the four cluster-bound cysteines are labeled. Spectrum has been recorded at 500 MHz, 298 K.

in the HNCA experiment and HN of Cys47 is not observed at all. Both Cys22 and Cys47 HN are observable in the paramagnetic ^{15}N-HSQC only at very short INEPT transfer delays, indicating that the HN vector is, in these cases, pointing towards the cluster.

3.3. Relaxation rates as assignment tools

The two $_{\beta}CH_2$ protons of Cys25 and Cys47 can be, finally assigned by analyzing the relaxation rates of H_β protons, measured from a ^{13}C IR-HSQC-AP experiment. Indeed, the ^{13}C HSQC-AP shows the $_{\beta}CH_2$ groups (Fig. 3**B**) of Cys25 and Cys47 that are not yet sequence specifically assigned. An Inversion Recovery building block, applied on top of a ^{13}C HSQC experiment, allows us to measure R_1 rates of the H_β protons, in analogy with what was already done for the ^{15}N HSQC-AP case [49]. Measured R_1 ^{1}H rates are 313 s^{-1} and 282 s^{-1} for the two protons bound to the C_β at 103.8 ppm, while the two protons bound to the C_β at 88.3 ppm show rates of 450 s^{-1} and 130 s^{-1}. Conversion of R_1 ^{1}H rates into upper distance limits gives metal-to-proton distances of 3.8 Å and 3.9 Å for the two protons bound to the C_β at 103.8 pm, while the two protons bound to the C_β at 88.3 ppm have metal-to-proton distances of 3.6 Å and 4.5 Å. These data show that Cys25 and Cys47 have different binding topologies: while in one case the two $_{\beta}CH_2$ protons are equally distant from the iron ion, in the other case the germinal $_{\beta}CH_2$ has a strong asymmetry, with one proton "facing" the iron ion at a short distance and the other one being about 0.9 Å farther. The X-ray and the NMR structures of the many HiPIPs characterized so far show that the cluster binding topologies are well conserved throughout the very many HiPIPs of known structure [81–84]. Indeed, the χ_2 dihedral angle of CysII (the second in the cluster binding sequence), which in the case of PioC is Cys25, is such that we expect two very similar metal-to-proton distances for the two Cys25 H_β protons. In the case of CysIV, which in PioC is Cys47, the χ_2 dihedral angle is such that $_{\beta}CH_2$ protons are quite asymmetric with respect to the iron ion, with one H_β close to the cluster and the other much farther apart. The symmetrical βCH_2 group (C_β at 103.8 ppm) is therefore assigned to Cys25 while $_{\beta}CH_2$ protons with asymmetric distances (C_β at 88.3 ppm) are assigned to Cys47.

The assignment is also supported by the hyperfine shift values experienced by each of the eight $_{\beta}CH_2$ protons. It is well known that hyperfine shifts of $_{\beta}CH_2$ protons of cysteine residues bound to a $[Fe_4S_4]^{2+}$ cluster depend on χ_2 dihedral angle, according to a Karplus-like relationship [85,86]. According to this model and to the pattern of shifts observed throughout several reduced HiPIPs, the $_{\beta}CH_2$ pair at ca. 10 and 8.0 ppm is likely to be attributed to Cys25, in agreement with the assignment via relaxation rates [76].

4. Discussion

The procedure for the assignment of cysteine residues bound to a paramagnetic center can be summarized in the color-coded Table 1. The sequence specific assignment, performed using the standard set of triple resonance experiments, leaves unassigned fragments: Cys22-Phe28, Ile35-Val37 and Cys47-Ala51. These regions encompass the four cysteine residues binding the 4Fe-4S cluster (Cys22, Cys25, Cys34 and Cys47) and the three amino acids following each of these. Therefore, the sequence specific assignment approach leaves Table 1 completely blank and sets the stage for a non-systematic approach to the assignment. The paramagnetic HNCA constituted the link between the residues assigned with the standard experiments and backbone resonance of cluster bound cysteines, thus providing, via the link with the HN of the following residue, the assignment of three out of four Cys C_α carbons (yellow). In turn, ^{13}C HSQC correlate each C_α with the corresponding Hα (orange). The ^{13}C HSQC also clearly identifies the four $_{\beta}CH_2$ of cluster-bound cysteines, two of them can be assigned thanks to 1D NOE experiments (green). ^{13}C–^{13}C COSY and CON allows to complete the assignment of N and C_α, providing the assignment of missing resonances from Cys47 (blue). Indeed, due to cysteine residues'

Table 1
Sequence-Specific Assignment of cysteine resonances. Table legend indicates the experiment used to assign each signal.

	Chemical shift (ppm)							
	HN	N	Cα	Hα	Cβ	$Hβ_1$	$Hβ_2$	CO
Cys22	9.47[a]	131.4[a]	89.5[a]	8.18[b]	102.65[c]	6.6[c]	16.6[c]	177.6[d]
Cys25	8.36[a]	130.3[a]	80.0[a]	3.82[b]	103.8[f]	8.09[f]	9.94[f]	176.5[d]
Cys34	8.55[a]	129.1[a]	90.3[a]	3.83[b]	111.1[c]	5.8[c]	14.5[c]	173.9[d]
Cys47	6.50[e]	118.8[d]	90.3[d]		88.3[f]	7.99[f]	8.95[f]	170.7[d]

a: HNCA. b: ^{13}C-HSQC. c: 1D-NOE and ^{13}C-HSQC d: ^{13}C-^{13}C COSY and CON e: ^{15}N-HSQC. f: Relaxation rates.

topology, the Cys47 H_N amide nitrogen is too close to the metal center and therefore the corresponding connectivity in an HNCA experiment would be lost. However, the CON is an efficient complement of the above experiment: when the polarization transfer from backbone H_N is not feasible due to fast R_2 relaxation of H_N signal, the polarization transfer from the preceding C' residue is an "alternative route" that makes possible the assignment of Cys47 N signal. Once Cys47 N has been assigned, the ^{15}N-HSQC shows a, yet unassigned, HN peak consistent with the Cys47 N shift, which is therefore attributed to Cys47 HN (red). Finally, the analysis of relaxation rates and considerations on the topology of Cys binding residues contribute to complete the puzzle and to assign Cys25 and Cys47 $_{\beta}CH_2$ (brown).

Although this analysis cannot be performed in an automated or semi-automated approach, the assignment is unambiguous and solid. Each individual assignment is supported by clear and consistent scalar and dipolar connectivities. The detectability of these connectivities is critically dependent on the relaxation properties of the system. Therefore, it is not possible to provide an "assignment protocol" that can be systematically used in different paramagnetic systems. For each chromophore and each binding residue, the interplay between the delays needed for the various coherence transfers and the relaxation rates of concerned resonances determines the best route to assign each signal.

Another interesting feature that can be exploited to obtain hints for the assignment and structural information in paramagnetic proteins, is the unpaired spin delocalization that may occur via hydrogen bonds. It is known that the network of hydrogen bonds around an iron-sulfur cluster plays a crucial role in stabilizing the cluster within the protein frame and in determining its reduction potential [87,88]. Fig. 7 reports the chemical shift differences between the ^{15}N shifts values observed in PioC and those expected according the average ^{15}N values reported in the BMRB data base [89]. There are three ^{15}N shift values that are outliers by more than 20 ppm with respect to the average values. This is only consistent with the presence of three hydrogen bonds that involve peptide HN of Gln27, Val37 and Leu49. Indeed, the NMR structure of PioC [90] confirms that Sγ of Cys25, Cys34, Cys47 are amenable to act as acceptors of hydrogen bonds from the above HN groups. This provides an additional path for the unpaired spin density delocalization from the metal center towards protein residues. This effect is weaker with respect to the electron density spin delocalization occurring via sigma bonds, however the observed shifts provide a direct, rare, experimental evidence of the way in which hydrogen bonds are involved into the highest occupied molecular orbitals of the chromophore.

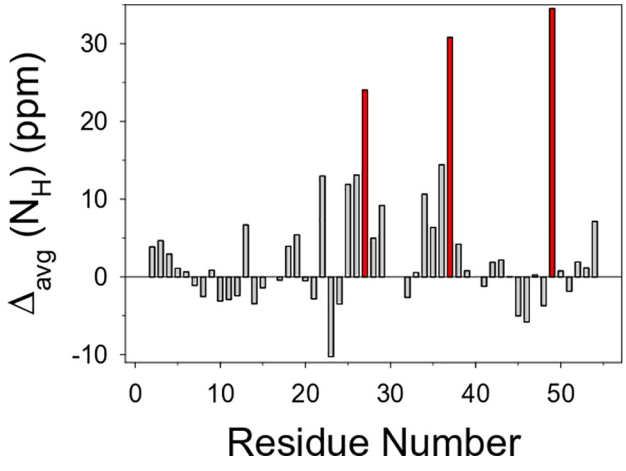

Fig. 7. Chemical shift differences between ^{15}N shift values observed in PioC and average aminoacid values, as reported in the Biological Magnetic Resonance Data Bank (http://www.bmrb.wisc.edu/ref_info/statful.htm). Residues whose ^{15}N shift values are outliers by more than 20 ppm with respect to the average values (Gln27, Val37 and Leu49) are shown in red. (For interpretation of the references to color in this figure legend, the reader is referred to the web version of this article.)

5. Concluding remarks

Paramagnetic NMR is nowadays a wide research field, covering a variety of important problems in chemistry and biology including catalysts, battery materials, metalloproteins and large protein–protein assemblies [21,42,91,92]. We have shown here that paramagnetic NMR is also a *fil-rouge* connecting coordination chemistry to structural biology, via advancements of knowledge and of investigation tools. The contribution of the hyperfine interaction to chemical shift and nuclear relaxation has been first addressed by coordination chemists. About half a century after the first successful applications of paramagnetic probes in biological chemistry [10,93–97], the subject has been periodically revisited and re-interpreted [30,98–100] to address structural and functional properties in biological systems and biomedicine. NMR of paramagnetic systems essentially contributed in providing a cross-over between inorganic chemistry and biochemistry and played a fundamental role in the development of Biological Inorganic Chemistry [101–109].

As far as Iron-Sulfur proteins are concerned, a longstanding major interest of the bio-inorganic chemistry community is the understanding at the molecular level of the way proteins of the iron-sulfur cluster assembly cellular machineries interact with one another, and how these machineries assemble different FeS clusters and deliver them to target proteins with high efficiency and specificity [110–113]. Typically, proteins involved into these processes are of large molecular size, difficult to isolate and purify, poorly soluble, thermodynamically unstable and driven by weak and transient interactions. In this scenario, small and stable proteins like PioC can be viewed as model systems that allow biophysicists to design and validate new experimental approaches that could eventually become useful to understand structure and dynamics of more complex systems.

The complete assignment of cysteine residues, including the elusive nuclei that could be detected and assigned only with this protocol, will be the ground for a systematic study of the relaxation properties of cysteine residues bound to $[Fe_4S_4]^{2+}$ cluster. There is work in progress for the detailed quantitative understanding of all factors contributing to transverse and longitudinal nuclear relaxation in the proximity of a paramagnetic center [43,44,114,115]. A $[Fe_4S_4]^{2+}$ cluster has unique properties in terms of electronic structures and, at the same time, is a common inorganic protein cofactor; we expect that accurate relaxation rates of all active spins of the cysteine residues will provide further information on the electron and nuclear relaxation properties in the system.

CRediT authorship contribution statement

Inês B. Trindade: Visualization, Investigation. **Michele Invernici:** Visualization, Investigation. **Francesca Cantini:** Software, Validation, Formal analysis, Writing - original draft, Writing - review & editing. **Ricardo O. Louro:** Writing - review & editing. **Mario Piccioli:** Conceptualization, Writing - original draft, Writing - review & editing.

Declaration of Competing Interest

The authors declare that they have no known competing financial interests or personal relationships that could have appeared to influence the work reported in this paper.

Acknowledgements

This work benefited from access to CERM/CIRMMP, the Instruct-ERIC Italy centre. Financial support was provided by European EC Horizon 2020 TIMB3 (Project 810856) Instruct-ERIC (PID 4509). This article is based upon work from COST Action CA15133, supported by COST (European Cooperation in Science and Technology). Fondazione Ente Cassa di Risparmio di Firenze (CRF 2016 0985) is acknowledged for providing fellowship to MI. This work was funded by national funds through FCT– Fundação para a Ciência e a Tecnologia, I.P., Project MOSTMICRO-ITQB with refs UIDB/04612/2020 and UIDP/04612/2020, and Fundação para a Ciência e a Tecnologia (FCT) Portugal is acknowledged for Grant PD/BD/135187/2017 to IBT.

References

[1] L. Sacconi, I. Bertini, J. Am. Chem. Soc. 88 (1966) 5180–5185.
[2] J.D. Thwaites, I. Bertini, L. Sacconi, Inorg. Chem. 5 (1966) 1036–1041.
[3] J.D. Thwaites, L. Sacconi, Inorg. Chem. 5 (1966) 1029–1035.
[4] G.N. La Mar, L. Sacconi, J. Am. Chem. Soc. 90 (1968) 7216–7223.
[5] G.N. La Mar, W.D. Horrocks Jr., L.C. Allen, J. Chem. Phys. 41 (1964) 2126–2134.
[6] R.H. Holm, G.W. Everett, W.D. Horrocks Jr., J. Am. Chem. Soc. 88 (1966) 1071.
[7] W.D. Horrocks Jr., D.D. Hall, Inorg. Chem. 10 (1971) 2368–2370.
[8] D.R. Eaton, R.D. Fischer, C.J. Hawkins, W.D. Horrocks Jr., J.P. Jesson, R.W. Kreilick, R.J. Kurland, G.N. La Mar, C.H. Langford, W.D. Phillips, L.H. Pignolet, M.F. Rettig, T.J. Swift, NMR of Paramagnetic Molecules, Academic Press, New York, 1973.
[9] I. Bertini, C. Luchinat, NMR of paramagnetic molecules in biological systems, Benjamin/Cummings, Menlo Park, CA, 1986.
[10] C.D. Barry, A.C.T. North, J.A. Glasel, R.J.P. Williams, A.V. Xavier, Nature 232 (1971) 236–245.
[11] E. Ab, A.R. Atkinson, L. Banci, I. Bertini, S. Ciofi-Baffoni, K. Brunner, T. Diercks, V. Dötsch, F. Engelke, G. Folkers, C. Griesinger, W. Gronwald, H. Gunther, M. Habeck, R. de Jong, H.R. Kalbitzer, B. Kieffer, B.R. Leeflang, S. Loss, C. Luchinat, T. Marquardsen, D. Moskau, K.P. Neidig, M. Nilges, M. Piccioli, R. Pierattelli, W. Rieping, T. Schippmann, H. Schwalbe, G. Trave, J.M. Trenner, J. Wohnert, M. Zweckstetter, R. Kaptein, Acta Crystallogr. D Biol. Crystallogr. 62 (2006) 1161.
[12] M. Mori, B. Jiménez, M. Piccioli, A. Battistoni, M. Sette, Biochemistry 47 (2008) 12954–12963.
[13] P. Serrano, S.K. Dutta, A. Proudfoot, B. Mohanty, L. Susac, B. Martin, M. Geralt, L. Jaroszewski, A. Godzik, M. Elsliger, I.A. Wilson, K. Wuthrich, FEBS J. (2016).
[14] A. Bax, G.M. Clore, J. Magn. Reson. 306 (2019) 187–191.
[15] F. Arnesano, L. Banci, I. Bertini, I.C. Felli, C. Luchinat, A.R. Thompsett, J. Am. Chem. Soc. 125 (2003) 7200–7208.
[16] S. Balayssac, B. Jiménez, M. Piccioli, J. Biomol. NMR 34 (2006) 63–73.
[17] M. Piccioli, P. Turano, Coord. Chem. Rev. 284 (2015) 313–328.
[18] W. Bermel, I. Bertini, I.C. Felli, M. Piccioli, R. Pierattelli, Progr. NMR Spectrosc. 48 (2006) 25–45.
[19] I. Solomon, Phys. Rev. 99 (1955) 559–565.
[20] M.A. Hass, M. Ubbink, Curr. Opin. Struct. Biol. 24 (2014) 45–53.
[21] A.J. Pell, G. Pintacuda, C.P. Grey, Prog. Nucl. Magn. Reson. Spectrosc. 111 (2019) 1–271.
[22] J.L. Battiste, G. Wagner, Biochemistry 39 (2000) 5355–5365.
[23] L.W. Donaldson, N.R. Skrynnikov, W.-Y. Choy, D.R. Muhandiram, B. Sarkar, J.D. Forman-Kay, L.E. Kay, J. Am. Chem. Soc. 123 (2001) 9843–9847.
[24] J.D. Gross, N.J. Moerke, T. von der Haar, A.A. Lugovskoy, A.B. Sachs, J.E.G. McCarthy, G. Wagner, Cell 115 (2003) 739–750.
[25] J. Iwahara, D.E. Anderson, E.C. Murphy, G.M. Clore, J. Am. Chem. Soc. 125 (2003) 6634–6635.
[26] W.-M. Liu, M. Overhand, M. Ubbink, Coord. Chem. Rev. 273–274 (2014) 2–12.
[27] E.C. Cetiner, H.R.A. Jonker, C. Helmling, D.B. Gophane, C. Grunewald, S.T. Sigurdsson, H. Schwalbe, J. Biomol. NMR 73 (2019) 699–712.
[28] G.M. Clore, J. Iwahara, Chem. Rev. 109 (2009) 4108–4139.
[29] N.J. Anthis, G.M. Clore, Q. Rev. Biophys. 48 (2015) 35–116.
[30] J. Iwahara, G.M. Clore, Nature 440 (2006) 1227–1230.
[31] T.P. Roosild, J. Greenwald, M. Vega, S. Castronovo, R. Riek, S. Choe, Science 307 (2005) 1317.
[32] C.W. Bertoncini, Y.-S. Jung, C.O. Fernández, W. Hoyer, C. Griesinger, T.M. Jovin, M. Zweckstetter, PNAS 102 (2005) 1430–1435.
[33] M.M. Dedmon, K. Lindorff-Larsen, J. Christodoulou, M. Vendruscolo, C.M. Dobson, J. Am. Chem. Soc. 127 (2005) 476–477.
[34] D.J. Felitsky, M.A. Lietzow, H.J. Dyson, P.E. Wright, Proc. Natl. Acad. Sci. 105 (2008) 6278.
[35] C.A. Softley, M.J. Bostock, G.M. Popowicz, M. Sattler, J. Biomol. NMR (2020).
[36] T. Muntener, D. Haussinger, P. Selenko, F.X. Theillet, J. Phys. Chem. Lett. 7 (2016) 2821–2825.
[37] B. Liang, J.H. Bushweller, L.K. Tamm, J. Am. Chem. Soc. 128 (2006) 4389–4397.
[38] L. Benda, J. Mare, E. Ravera, G. Parigi, C. Luchinat, M. Kaupp, J. Vaara, Angew. Chem. Int. Ed. 5 (2016) 14713–14717.
[39] E.A. Suturina, I. Kuprov, PCCP 18 (2016) 26412–26422.
[40] S.A. Rouf, J. Mareš, J. Vaara, J. Chem. Theory Comput. 11 (2015) 1683–1691.
[41] P.J. Cherry, S.A. Rouf, J. Vaara, J. Chem. Theory Comput. 13 (2017) 1275–1283.
[42] E.A. Suturina, K. Mason, C. Geraldes, N.F. Chilton, D. Parker, I. Kuprov, PCCP 20 (2018) 17676–17686.
[43] D. Parker, E.A. Suturina, I. Kuprov, N.F. Chilton, Acc. Chem. Res. (2020).
[44] H.W. Orton, G. Otting, J. Am. Chem. Soc. 140 (2018) 7688–7697.
[45] H.W. Orton, I. Kuprov, C.-T. Loh, G. Otting, J. Phys. Chem. Lett. 7 (2016) 4815–4818.
[46] G. Pintacuda, A. Kaikkonen, G. Otting, J. Magn. Reson. 171 (2004) 233–243.
[47] G. Pintacuda, K. Hohenthanner, G. Otting, N. Muller, J. Biomol. NMR 27 (2003) 115–132.
[48] D.F. Hansen, J.J. Led, J. Am. Chem. Soc. 126 (2004) 1247–1252.
[49] S. Ciofi-Baffoni, A. Gallo, R. Muzzioli, M. Piccioli, J. Biomol. NMR 58 (2014) 123–128.
[50] M. Invernici, I.B. Trindade, F. Cantini, R.O. Louro, M. Piccioli, J. Biomol. NMR (2020).
[51] L. Banci, I. Bertini, V. Calderone, S. Ciofi-Baffoni, A. Giachetti, D. Jaiswal, M. Mikolajczyk, M. Piccioli, J. Winkelmann, PNAS 110 (2013) 7136–7141.
[52] L. Banci, D. Brancaccio, S. Ciofi-Baffoni, R. Del Conte, R. Gadepalli, M. Mikolajczyk, S. Neri, M. Piccioli, J. Winkelmann, PNAS 111 (2014) 6203–6208.
[53] G. Van Driessche, I. Vandenberghe, B. Devreese, B. Samyn, T.E. Meyer, R. Leigh, M.A. Cusanovich, R.G. Bartsch, U. Fischer, J.J. Van Beeumen, J. Mol. Evol. 57 (2003) 181–199.
[54] I.B. Trindade, M. Invernici, F. Cantini, R.O. Louro, M. Piccioli, Biomol. Nmr. Assign (2020).
[55] I. Bertini, B. Jiménez, M. Piccioli, J. Magn. Reson. 174 (2005) 125–132.
[56] T. Inubushi, E.D. Becker, J. Magn. Reson. 51 (1983) 128–133.
[57] S. Ramaprasad, R.D. Johnson, G.N. La Mar, J. Am. Chem. Soc. 106 (1984) 5330–5335.
[58] L. Banci, I. Bertini, C. Luchinat, M. Piccioli, A. Scozzafava, P. Turano, Inorg. Chem. 28 (1989) 4650–4656.
[59] I. Bertini, B. Jiménez, M. Piccioli, L. Poggi, J. Am. Chem. Soc. 127 (2005) 12216–12217.
[60] I. Bertini, Y.-M. Lee, C. Luchinat, M. Piccioli, L. Poggi, ChemBioChem 2 (2001) 550–558.
[61] U. Kolczak, J. Salgado, G. Siegal, M. Saraste, G.W. Canters, Biospectroscopy 5 (1999) S19–S32.
[62] M. Kostic, S.S. Pochapsky, T.C. Pochapsky, J. Am. Chem. Soc. 124 (2002) 9054–9055.
[63] T.E. Machonkin, W.M. Westler, J.L. Markley, J. Am. Chem. Soc. 124 (2002) 3204–3205.
[64] I. Bertini, L. Duma, I.C. Felli, M. Fey, C. Luchinat, R. Pierattelli, P.R. Vasos, Angew. Chem. Int. Ed. 43 (2004) 2257–2259.
[65] F. Arnesano, L. Banci, M. Piccioli, Q. Rev. Biophys. 38 (2005) 167–219.
[66] I. Gelis, N. Katsaros, C. Luchinat, M. Piccioli, L. Poggi, Eur. J. Biochem. 270 (2003) 600–609.
[67] V. Thanabal, J.S. de Ropp, G.N. La Mar, J. Am. Chem. Soc. 108 (1986) 4244–4245.
[68] R.O. Louro, I. Pacheco, D.L. Turner, J. LeGall, A.V. Xavier, FEBS Lett. 390 (1996) 59–62.
[69] B.J. Goodfellow, A.L. Macedo, P. Rodrigues, I. Moura, V. Wray, J.J.G. Moura, J. Biol. Inorg. Chem. 4 (1999) 421–430.
[70] N.V. Shokhirev, F.A. Walker, J. Phys. Chem. 99 (1995) 17795–17804.
[71] J.D. Satterlee, J.E. Erman, Arch. Biochem. Biophys. 202 (1980) 608–616.
[72] S. Vathyam, R.A. Byrd, A.F. Miller, J. Biomol. NMR 14 (1999) 293–294.
[73] M.D. Liptak, X. Wen, K.L. Bren, J. Am. Chem. Soc. 132 (2010) 9753–9763.
[74] M. Rivera, G.A. Caignan, Anal. Bioanal. Chem. 378 (2004) 1464–1483.
[75] N. Goasdoue, D.G. Riviere, I. Correia, O. Convert, M. Piccioli, Magn. Reson. Chem. 38 (2000) 827–832.
[76] I. Bertini, F. Capozzi, C. Luchinat, M. Piccioli, M. Vicens Oliver, Inorg. Chim. Acta 198-200 (1992) 483–491.
[77] A. Piai, T. Hošek, L. Gonnelli, A. Zawadzka-Kazimierczuk, W. Kozminski, B. Brutscher, W. Bermel, R. Pierattelli, I.C. Felli, J. Biomol. NMR 60 (2014) 209–218.
[78] M. Mori, F. Kateb, G. Bodenhausen, M. Piccioli, D. Abergel, J. Am. Chem. Soc. 132 (2010) 3594–3600.
[79] C. Caillet-Saguy, M. Delepierre, A. Lecroisey, I. Bertini, M. Piccioli, P. Turano, J. Am. Chem. Soc. 128 (2006) 150–158.

[80] D.L. Turner, R.J.P. Williams, Eur. J. Biochem. 211 (1993) 555–562.
[81] Y. Hirano, K. Takeda, K. Miki, Nature 534 (2016) 281–284.
[82] M. Stelter, A.M. Melo, S. Hreggvidsson, L.M. Saraiva, M. Teixeira, M. Archer, J. Biol. Inorg. Chem. 15 (2010) 303–313.
[83] L. Banci, I. Bertini, L.D. Eltis, I.C. Felli, D.H.W. Kastrau, C. Luchinat, M. Piccioli, R. Pierattelli, M. Smith, Eur. J. Biochem. 225 (1994) 715–725.
[84] I. Rayment, G. Wesenberg, T.E. Meyer, M.A. Cusanovich, H.M. Holden, J. Mol. Biol. 228 (1992) 672–686.
[85] I. Bertini, F. Capozzi, C. Luchinat, M. Piccioli, A.J. Vila, J. Am. Chem. Soc. 116 (1994) 651–660.
[86] E.W. Stone, A.H. Maki, J. Chem. Phys. 37 (1962) 1326–1333.
[87] J.A. Birrell, C. Laurich, E.J. Reijerse, H. Ogata, W. Lubitz, Biochemistry 55 (2016) 4344–4355.
[88] I.J. Lin, E.B. Gebel, T.E. Machonkin, W.M. Westler, J.L. Markley, PNAS 102 (2005) 14581–14586.
[89] E.L. Ulrich, H. Akutsu, J.F. Doreleijers, Y. Harano, Y.E. Ioannidis, J. Lin, M. Livny, S. Mading, D. Maziuk, Z. Miller, E. Nakatani, C.F. Schulte, D.E. Tolmie, R.K. Wenger, H. Yao, J.L. Markley, Nucleic Acids Res. 36 (2008) D402–D408.
[90] I.B. Trindade, M. Invernici, F. Cantini, R.O. Louro, M. Piccioli, Submitted.
[91] J. Kowalewski, P.H. Fries, D. Kruk, M. Odelius, A.V. Egorov, S. Krämer, H. Stork, M. Horvatić, C. Berthier, J. Magn. Reson. 314 (2020) 106737.
[92] J. Mares, J. Vaara, PCCP 20 (2018) 22547–22555.
[93] C.M. Dobson, R.J.P. Williams, A.V. Xavier, J. Chem. Soc., Dalton Trans. (1973) 2662.
[94] A.V. Xavier, E.W. Czerwinski, P.H. Bethge, F.S. Mathews, Nature 275 (1978) 245–247.
[95] B. Bleaney, C.M. Dobson, B.A. Levine, R.B. Martin, R.J.P. Williams, A.V. Xavier, J. Chem. Soc., Chem. Commun. (1972) 791.
[96] L. Lee, B.D. Sykes, Biochemistry 19 (1980) 3208–3214.
[97] C.D. Barry, C.M. Dobson, R.J.P. Williams, A.V. Xavier, J. Chem. Soc. Dalton Trans. (1974) 1765–1769.
[98] J.R. Tolman, J.M. Flanagan, M.A. Kennedy, J.H. Prestegard, PNAS 92 (1995) 9279–9283.
[99] N. Niccolai, O. Spiga, A. Bernini, M. Scarselli, A. Ciutti, I. Fiaschi, S. Chiellini, H. Molinari, P.A. Temussi, J. Mol. Biol. 332 (2003) 437–447.
[100] S. Aime, D. Delli Castelli, S. Geninatti Crich, E. Gianolio, E. Terreno, Acc. Chem. Res. 42 (2009) 822–831.
[101] G.W. Canters, H.A. Hill, N.A. Kitchen, E.T. Adman, Eur. J. Biochem. 138 (1984) 141–152.
[102] M. Ubbink, J.A.R. Worrall, G.W. Canters, E.J.J. Groenen, M. Huber, Annu. Rev. Biophys. Biomol. Struct. 31 (2002) 393–422.
[103] S.J. Lippard, A.R. Burger, K. Ugurbil, M.W. Pantoliano, J.S. Valentine, Biochemistry 16 (1977) 1136–1141.
[104] H. Toi, G.N. La Mar, R. Margalit, C.-M. Che, H.B. Gray, J. Am. Chem. Soc. 106 (1984) 6213–6217.
[105] R.B. Lauffer, L. Que Jr., J. Am. Chem. Soc. 104 (1982) 7324–7325.
[106] M.J. Maroney, D.M. Kurtz Jr., J.M. Nocek, L.L. Pearce, L. Que Jr., J. Am. Chem. Soc. 108 (1986) 6871–6879.
[107] R.K.O. Sigel, H. Sigel, Acc. Chem. Res. 43 (2010) 974–984.
[108] H. Santos, J.J.G. Moura, I. Moura, J. LeGall, A.V. Xavier, Eur. J. Biochem. 141 (1984) 283–296.
[109] R.O. Louro, I.J. Correia, L. Brennan, I.B. Coutinho, A.V. Xavier, D.L. Turner, J. Am. Chem. Soc. 120 (1998) 13240–13247.
[110] S. Adinolfi, C. Iannuzzi, F. Prischi, C. Pastore, S. Iametti, S.R. Martin, F. Bonomi, A. Pastore, Nat. Struct. Mol. Biol. 16 (2009) 390–396.
[111] T.A. Rouault, Nat. Rev. Mol. Cell Biol. 16 (2015) 45–55.
[112] M.A. Uzarska, V. Nasta, B.D. Weiler, F. Spantgar, S. Ciofi-Baffoni, M. Saviello, L. Gonnelli, U. Muhlenhoff, L. Banci, R. Lill, eLife 5 (2016) e16673.
[113] L. Banci, F. Camponeschi, S. Ciofi-Baffoni, M. Piccioli, J. Biol. Inorg. Chem. 23 (2018) 687.
[114] D.F. Hansen, W.M. Westler, M.B.A. Kunze, J.L. Markley, F. Weinhold, J.J. Led, J. Am. Chem. Soc. 134 (2012) 4670–4682.
[115] W. Andralojc, Y. Hiruma, W.-M. Liu, E. Ravera, M. Nojiri, G. Parigi, C. Luchinat, M. Ubbink, PNAS 114 (2017) E1840–E1847.